れた Colon-26 細胞由来のがん関連抗原を樹状細胞が取込み、リンパ節に移動して $CD8^+$ T 細胞を活性化し、Colon-26 細胞特異的 CTL の誘導により　抗腫瘍効果が発揮されていることが明示された。

D. 考察、

バブルリポソームを利用した超音波がん温熱療法を施したがん組織内に樹状細胞を投与することで、細胞性免疫を中心とした抗腫瘍免疫を効率よく誘導できることが明らかとなった（図４）。

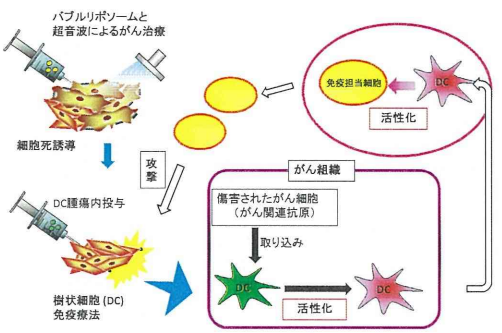

図４ バブルリポソームを利用した超音波がん温熱療法と樹状細胞免疫療法の併用によるがん治療戦略

E. 結論

バブルリポソームを利用した超音波がん温熱療法と樹状細胞免疫療法の併用は有効な抗腫瘍免疫を誘導可能であるため、新たながん治療戦略として利用可能になるものと期待される。

F. 健康危険情報

なし

G. 研究発表

１．論文発表

（英文論文のみ）

1. R Suzuki, Y Oda, D Omata, N Nishiie, R Koshima, Y Shiona, Y Sawaguchi, J Ung , T Naoi, Y Negishi, S Kawakami, M Hashida, K Maruyama Tumor growth suppression by mild hyperthermia using non-high intensity focused ultrasound in combination with nanobubbles. Int. Hyperthermia 2014 in press.

H. 知的財産権の出願・登録状況

なし

Cancer Science
The official journal of the Japanese Cancer Association

NC-6300, an epirubicin-incorporating micelle, extends the antitumor effect and reduces the cardiotoxicity of epirubicin

Amane Takahashi,[1,2,3] Yoshiyuki Yamamoto,[1,4] Masahiro Yasunaga,[1] Yoshikatsu Koga,[1] Jun-ichiro Kuroda,[1] Misato Takigahira,[1] Mitsunori Harada,[5] Hiroyuki Saito,[5] Tatsuyuki Hayashi,[5] Yasuki Kato,[5] Taira Kinoshita,[2] Nobuhiro Ohkohchi,[3] Ichinosuke Hyodo[4] and Yasuhiro Matsumura[1,6]

[1]Division of Developmental Therapeutics, Research Center for Innovative Oncology, Kashiwa; [2]Upper Abdominal Surgical Oncology, National Cancer Center Hospital East, Kashiwa; [3]Department of Surgery, Advanced Biomedical Applications, University of Tsukuba, Tsukuba; [4]Department of Gastroenterology and Hepatology, Institute of Clinical Medicine, Graduate School of Comprehensive Human Sciences, University of Tsukuba, Tsukuba; [5]Research Division, NanoCarrier Co. Ltd., Kashiwa, Japan

(Received January 4, 2013/Revised February 25, 2013/Accepted March 11, 2013/Accepted manuscript online March 16, 2013/Article first published online April 19, 2013)

Epirubicin is widely used to treat various human tumors. However, it is difficult to achieve a sufficient antitumor effect because of dosage limitation to prevent cardiotoxicity. We hypothesized that epirubicin-incorporating micelle would reduce cardiotoxicity and improve the antitumor effect. NC-6300 comprises epirubicin covalently bound to PEG polyaspartate block copolymer through an acid–labile hydrazone bond. The conjugate forms a micellar structure of 40–80 nm in diameter in an aqueous milieu. NC-6300 (10, 15 mg/kg) and epirubicin (10 mg/kg) were given i.v. three times to mice bearing s.c. or liver xenograft of human hepatocellular carcinoma Hep3B cells. Cardiotoxicity was evaluated by echocardiography in C57BL/6 mice that were given NC-6300 (10 mg/kg) or epirubicin (10 mg/kg) in nine doses over 12 weeks. NC-6300 showed a significantly potent antitumor effect against Hep3B s.c. tumors compared with epirubicin. Moreover, NC-6300 also produced a significantly longer survival rate than epirubicin against the liver orthotopic tumor of Hep3B. With respect to cardiotoxicity, epirubicin-treated mice showed significant deteriorations in fractional shortening and ejection fraction. In contrast, cardiac functions of NC-6300 treated mice were no less well maintained than in control mice. This study warrants a clinical evaluation of NC-6300 in patients with hepatocellular carcinoma or other cancers. (*Cancer Sci* 2013; 104: 920–925)

Hepatocellular carcinoma (HCC) is the fifth most common cancer and the third largest cause of cancer mortality worldwide.[1,2] The range of available oncological treatment for HCC is sometimes limited due to poor liver function caused by concomitant chronic liver disease, especially liver cirrhosis, which is mainly the result of hepatitis virus infection. Surgical resection is widely considered the mainstay for curative treatment and yields a certain survival rate. However, <20% of patients with HCC can undergo surgical resection.[3,4] With the exception of patients at an early stage and with adequate liver function, recurrence rates after surgical resection are unfortunately high. High recurrence rates are also seen in patients treated by other local treatment options, such as ablation, percutaneous ethanol injection, and trans-arterial chemoembolization.[5] For advanced HCC, the only available option is sorafenib, a tyrosine kinase inhibitor, which was recently approved; however, the survival rate associated with its use is far from satisfactory.[6–8]

Anthracyclines such as epirubicin (EPI) and doxorubicin (DXR) are widely used and highly effective anticancer agents for the treatment of various human tumors including HCC, breast cancer, and gastric cancer.[9–13] However, anthracyclines induce several adverse effects, among which acute or chronic cardiotoxicity sometimes causes patients irreversible damage.[14–17] Cardiotoxicity of EPI is approximately 66% of that of DXR, but it is still the most serious problem in oncological treatment; this side-effect can sometimes require cessation of EPI treatment, resulting in an insufficient antitumor effect.[18–20] To address these issues, various anthracyclines have been developed to reduce cardiotoxicity without loss of the antitumor effect. However, to date, no such anthracyclines are available in a clinical context.

Against this background, NC-6300 was synthesized. NC-6300 comprises EPI covalently bound to PEG polyaspartate block copolymer through an acid–labile hydrazone bond. The conjugate spontaneously forms a micellar structure with a diameter of 40–80 nm in aqueous media, as reported previously.[21] *In vitro* findings indicated that it showed pH-dependent EPI release, namely, the release of EPI from NC-6300 accelerated under increasingly acidic conditions. NC-6300 is stable in the bloodstream for a long time; therefore, it accumulates selectively in tumor tissues through the enhanced permeability and retention effect.[21,22] Following the extravasation of NC-6300, NC-6300 or its disintegrated EPI-bound unimers reach and enter cancer cells. Then, under the acidic conditions within lysosomes, EPI may be released, leading to the subsequent death of the cancer cells.

In this study, we evaluated the antitumor effect of NC-6300 using mouse models with human HCC Hep3B cells. Moreover, we examined the cardiotoxicity of NC-6300, particularly in terms of cardiac function, by using echocardiography over a long period.

Materials and Methods

Drugs. NC-6300 was supplied and synthesized by NanoCarrier (Kashiwa, Japan) (Fig. 1). The synthesis was described elsewhere.[21] NC-6300 was stored in a frozen state at −80°C and melted on ice immediately before inoculation into mice. Then, the NC-6300 was prepared with distilled water at 1.0 mg/mL (epirubicin-equivalent dose). NC-6300 is stable at low temperatures under neutral conditions, but gradually begins to release the encapsulated EPI in an acidic environment.[21] The EPI was purchased from Pfizer Japan (Tokyo, Japan).

Cell culture. The human HCC cell line Hep3B was obtained from the European Collection of Cell Culture (ECACC, Salis-

[6]To whom correspondence should be addressed.
E-mail: yhmatsum@east.ncc.go.jp

doi: 10.1111/cas.12153

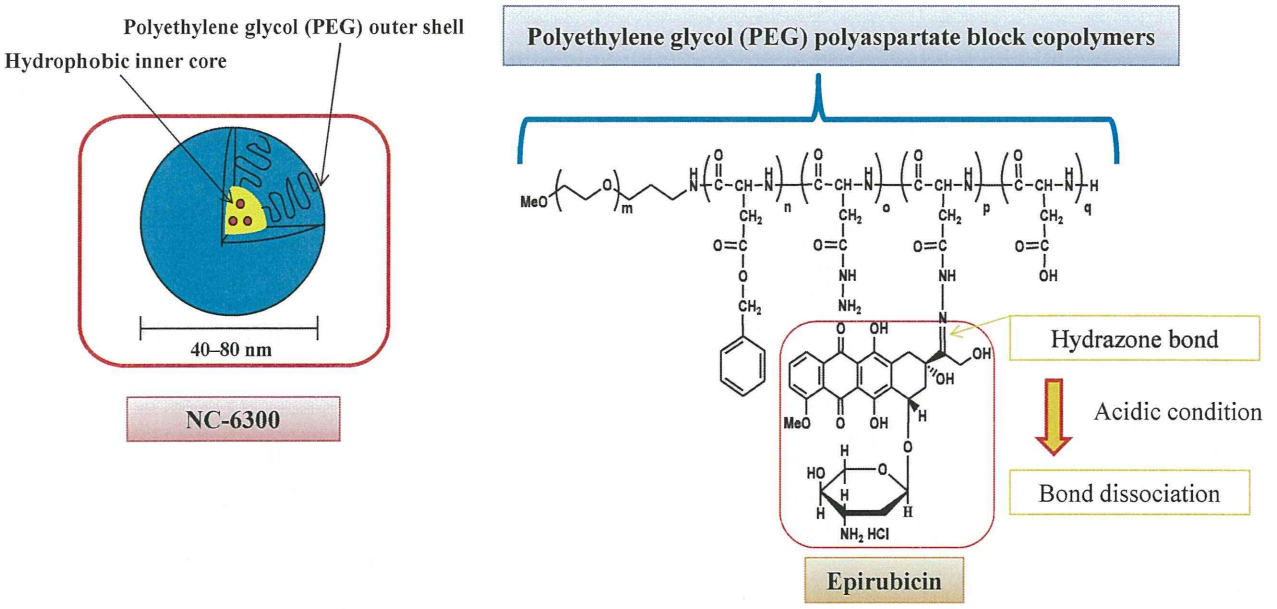

Fig. 1. NC-6300 comprises epirubicin covalently bound to the polyaspartate chain of PEG polyaspartate block copolymer by an acid–labile hydrazone bond. The conjugate spontaneously forms a micellar structure in an aqueous milieu. The diameter of NC-6300 is 40–80 nm, and the micellar formulation is stable under physiological conditions.

bury, UK). Hep3B cells were cultured in DMEM supplemented with 10% FBS (Cell Culture Technologies, Gaggenau-Hoerden, Germany), penicillin, streptomycin, and amphotericin B (100 units/mL, 100 μg/mL, and 25 μg/mL, respectively; Sigma, St. Louis, MO, USA) in humidified 5% CO_2 at 37°C.

Establishment of Hep3B cell line stably expressing firefly luciferase. For the *in vivo* bioluminescence imaging of liver orthotopic tumors, the Hep3B cell line stably expressing firefly luciferase (Hep3B/Luc) was established. Briefly, the coding sequence for firefly luciferase was subcloned into the pcDNA3.1(+) vector (Invitrogen, Carlsbad, CA, USA) to generate plasmids of pcDNA3.1/luciferase. Hep3B cells (2×10^5) were seeded onto 3-cm dishes 24 h before transfection. The cells were transfected with 2.5 μg plasmid DNA using Lipofectamine LTX Reagent and PLUS Reagent (Invitrogen) in accordance with the manufacturer's instructions, then incubated for 48 h at 37°C. The cells were then passaged in medium containing G418 (1 mg/mL; Invitrogen) to select for the neomycin-resistance gene integrated in the pcDNA3.1(+) plasmids. The accuracy of a quantitative bioluminescence image as an indicator of Hep3B/Luc cell number was analyzed using the IVIS Kinetic Imaging system (Caliper Life Sciences, Hopkinton, MA, USA) *in vitro*, as described below. This analysis showed a clear correlation between a quantitative bioluminescence image and cell number. The sensitivity of Hep3B/Luc cells to each anticancer drug was similar to that of parental Hep3B cells (data not shown).

Orthotopic tumor model. Six- to eight-week-old female BALB/c nude mice (CLEA Japan, Tokyo, Japan) each weighing approximately 20 g at the time of surgery were used for *in vivo* studies. The animals were maintained under specific pathogen-free conditions in cages, provided with standard food, and given free access to sterilized water. All animal procedures were carried out in compliance with the Guidelines for the Care and Use of Experimental Animals established by the Committee for Animal Experimentation of the National Cancer Center, Japan; these guidelines meet the ethical standards required by law and also comply with the guidelines for the use of experimental animals in Japan.

The HCC model was created by direct intrahepatic inoculation of Hep3B/Luc cells. The mice were anesthetized by i.p. injection of 0.15 mL/g body weight of 2,2,2-tribromoethanol in 2-methyl-2-butanol. The stock solution of the anesthetic is 1.0 g 2,2,2-tribromoethanol (Wako, Osaka, Japan) dissolved in 1.0 mL 2-methyl-2-butanol (Sigma). Just before use, 1 mL stock solution was diluted with 40 mL H_2O. A short median laparotomy was carried out with disinfection of the abdominal skin. Then, 5×10^6 Hep3B/Luc cells suspended in 20 μL Matrigel (BD Biosciences, San Jose, CA, USA) were directly injected into the left lower lobe of the liver using a 29-gauge needle. To prevent either bleeding or dissemination of tumor cells, puncture sites were ablated with a bipolar cautery.

***In vivo* tumor growth inhibition assay.** *Experiment 1.* Six-week-old BALB/c nude mice (CLEA Japan) were s.c. inoculated with 1×10^7 Hep3B/Luc cells in the flank region. When the tumor volume reached 150 mm^3, the mice were randomly divided into test groups consisting of six mice per group (day 0). Drug was given i.v. on days 0, 7, and 14 through the lateral tail vein. NC-6300 was given at 10 and 15 mg/kg and the reference drug, EPI, was given at its maximum tolerated dose of 10 mg/kg. The length (*a*) and width (*b*) of s.c. tumors and body weight were measured twice a week, and tumor volume (TV) was calculated as follows: $TV = (a \times b^2)/2$. Relative body weight (RBW) on day *n* was calculated according to the following formula: $RBW = BW_n/BW_0$, where BW_n is the body weight on day *n* and BW_0 is the body weight on day 0.

Experiment 2. Two weeks after direct hepatic inoculation of Hep3B/Luc cells, mice were randomly divided into three tests groups consisting of 10 mice per group (day 0). Randomization was carried out on the basis of bioluminescence images, and we confirmed that the mean values of count per minute in the images were not significantly different between groups. The mice were given i.v. injections into the lateral tail vein (200 μL) at 10 mg/kg or 15 mg/kg NC-6300, or 10 mg/kg

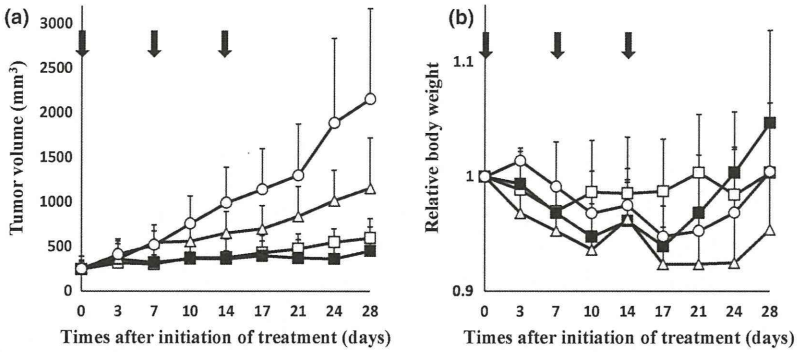

Fig. 2. Antitumor effects of NC-6300 and epirubicin (EPI) in mice bearing s.c. Hep3B xenografts. Hep3B cells (1×10^7 cells) were inoculated s.c. on the back. NC-6300 or conventional EPI was injected i.v. on days 0, 7, and 14. Day 0 indicates the day when tumor volume reached 150 mm^3 ($n = 6$). The dose of NC-6300 is expressed as dose equivalent of EPI. ○, Control; □, NC-6300 at 10 mg/kg; ■, NC-6300 at 15 mg/kg; △, EPI at 10 mg/kg. (a) Antitumor activity of NC-6300 or EPI was evaluated by measuring the tumor volume. The ANOVA test between NC-6300 (10 mg/kg) and EPI (10 mg/kg), $P = 0.0017$; NC-6300 (15 mg/kg) and EPI (10 mg/kg), $P < 0.001$. (b) Changes in relative body weight. Data were derived from the same mice as those used in the treatment experiment. The ANOVA test between NC-6300 (10 mg/kg) and EPI (10 mg/kg), $P = 0.0053$; NC-6300 (15 mg/kg) and EPI (10 mg/kg), $P < 0.001$. Arrows, drug injections; bars, SD; points, mean.

EPI, on days 0, 7, and 14. Control mice were injected with 200 μL PBS following the same schedule. To evaluate the progression of orthotopic liver tumor, *in vivo* bioluminescence imaging was carried out with the IVIS Kinetic Imaging system (Caliper Life Sciences) every week from the day of treatment initiation, and the body weight of each mouse was also measured. Mortality and morbidity were checked daily and the mice were maintained until each one showed signs of morbidity (massive ascites or hepatic tumor that could be observed through skin, jaundice, and 20% weight loss), at which point they were killed.

Pharmacokinetics of EPI and NC-6300 in mice. Four weeks after direct tumor inoculation of Hep3B/Luc in the liver, either EPI (10 mg/kg) or NC-6300 (10 mg/kg) was injected i.v. Before sampling, the mice were anesthetized with ether. Plasma, tumor, liver, heart, kidney, spleen, and lung were obtained and weighed at 1, 6, 12, 24, and 72 h. Tissue samples were rinsed with saline and stored at −80°C until use.

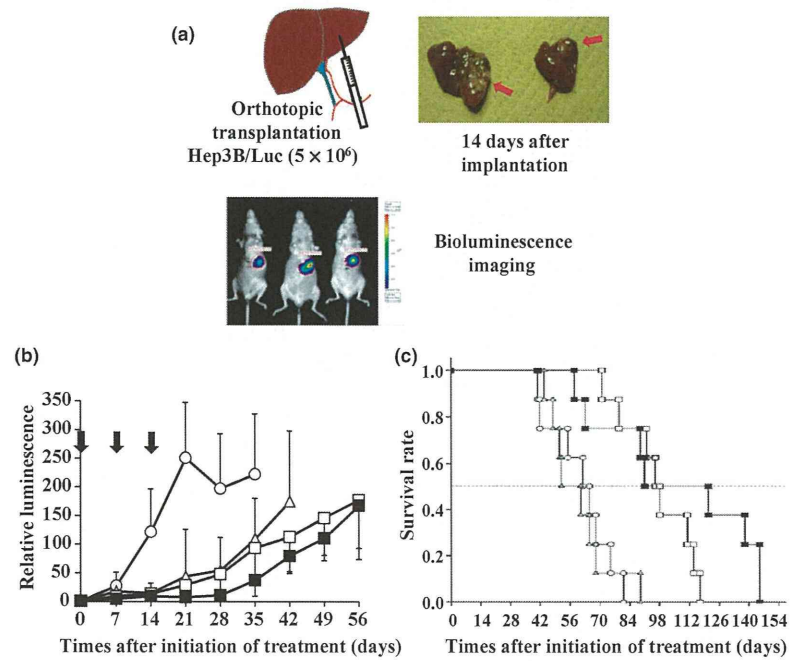

Fig. 3. (a) Orthotopic liver tumor xenografts and evaluation of tumor growth using bioluminescence imaging. Hep3B/Luc cells (5×10^6) suspended in 20 μL Matrigel were directly injected into the left lower lobe of the liver in mice using a 29-gauge needle. To visualize and evaluate the transplanted hepatic tumor of Hep3B/Luc cells, *in vivo* bioluminescence imaging was carried out. (b) Antitumor effect of NC-6300 and epirubicin (EPI) in mice bearing Hep3B/Luc xenografts. Each drug was given on days 0, 7, and 14 after tumor implantation ($n = 8$). The antitumor activity was evaluated by determining the relative photon count. The ANOVA test between NC-6300 (15 mg/kg) and EPI (10 mg/kg), $P = 0.025$. Arrows, drug injections; bars, SD; points, mean. (c) Kaplan–Meier curves. Log–rank test, NC-6300 (10 mg/kg) group *versus* EPI (10 mg/kg) group, $P = 0.002$; NC-6300 (15 mg/kg) group *versus* EPI (10 mg/kg) group, $P = 0.004$. ○, Control; □, NC-6300 at 10 mg/kg; ■, NC-6300 at 15 mg/kg; △, EPI at 10 mg/kg.

doi: 10.1111/cas.12153

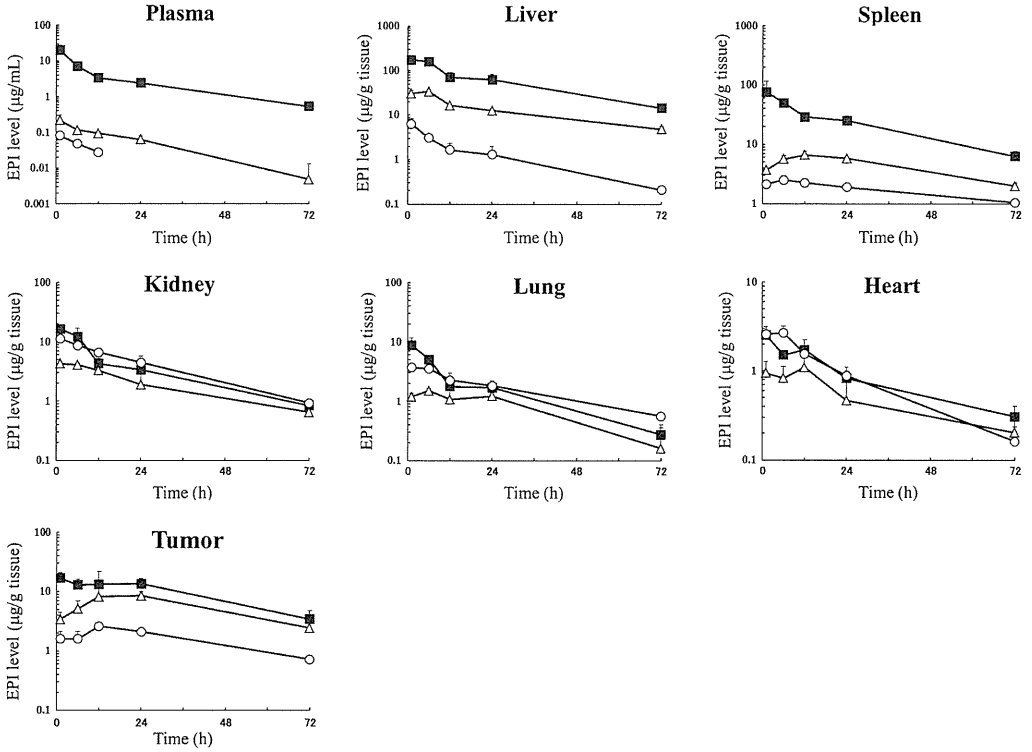

Fig. 4. Plasma and tissue concentration–time profiles of total (■) and released (Δ) epirubicin (EPI) after i.v. injection of NC-6300 (10 mg/kg) into mice bearing Hep3B/Luc orthotopic liver tumors. Plasma and tissue concentration–time profiles of EPI after conventional EPI (10 mg/kg) (○) injection. Data points are the means of three mice.

Table 1. Area under the time–concentration curve (AUC) values in plasma and tissues after injection of NC-6300 at 10 mg/kg or epirubicin (EPI) at 10 mg/kg in mice bearing orthotopic Hep3B/Luc liver xenografts

	AUC (μg/g tissue or mL × h)				
	NC-6300			Conventional EPI	Released/Conventional EPI AUC ratio
	Released EPI	Total EPI	% Released		
Plasma	4.1	213.0	1.9	0.6	6.95
Liver	920.5	4246.8	21.7	94.9	9.70
Spleen	323.3	1657.3	19.5	121.9	2.65
Kidney	136.2	273.5	49.8	295.2	0.46
Lung	61.4	127.2	48.3	118.7	0.52
Heart	36.2	63.7	56.9	66.9	0.54
Tumor	422.5	724.2	58.3	116.8	3.62

Tissue samples were suspended in 0.1 M sodium phosphate buffer (pH 7.4) at a concentration of 25% w/w and homogenized on ice using Precellys 24 (Bertin Technologies, Montigny-le-Bretonneux, France). Using aliquots of the homogenates and plasma (50 μL), concentrations of the EPI released from NC-6300 *in vivo* and the total EPI (free EPI released from NC-6300 *in vivo* and the polymer-bound EPI) were determined.

To determine the concentration of released EPI, the homogenates and plasma samples (50 μL) were treated with acetonitrile (125 μL) to precipitate proteins. Then, 1% Triton X-100 (25 μL) was added and the sample was vortexed and centrifuged for 5 min at 5000 *g* at 4°C. Subsequently, 75 μL daunorubicin HCL (2 μg/mL)/20 mM sodium phosphate buffer (pH 7.4) was added to the supernatant (75 μL) as an internal control. The prepared mixture was analyzed by HPLC. To determine the total EPI concentration, the samples (50 μL) were treated with acetonitrile (130 μL) and acidified with 1 N HCL (20 μL) for 1 h at room temperature to allow the complete release of EPI from NC-6300. Next, 1% Triton X-100 (25 μL) was added and the sample was vortexed and centrifuged for 5 min at 5000 *g* at 4°C. Then, 75 μL daunorubicin HCL (2 μg/mL)/25 mM ammonium formate buffer (pH 3.0) was added to the supernatant (75 μL) as an internal control. The prepared mixture was analyzed by HPLC.

Reversed-phase HPLC was carried out at 40°C on a Tosoh TSK-gel ODS-80Tm (4.6 ϕ × 150 mm; Tosoh, Tokyo, Japan) with a Tosoh ODS-80Tm guard cartridge. The EPI was eluted with 25 mM ammonium formate buffer (pH 3.0):acetonitrile (70:30, v/v) using a Waters Alliance System (Waters Corporation, Milford, MA, USA) at a flow rate of 1.0 mL/min. Detec-

tion was carried out using a Waters fluorescence detector with excitation and emission wavelengths of 488 and 560 nm, respectively.

Echocardiography for mice. To investigate the acute and chronic cardiotoxicity induced by EPI, we designed the following experimental scheme. Five-week-old female C57BL/6 mice were given NC-6300 at a dose of 10 mg/kg or EPI at 10 mg/kg (n = 6) on days 0, 7, and 14, and the mice were left for an interval of 7 days. We repeated this schedule three times; namely, mice were given each drug nine times in total. We evaluated the cardiac function using echocardiography on days 0, 7, 14, 21, 49, and 77.

Echocardiography was carried out using a high-resolution Micro Ultrasound system (Vevo 770; VisualSonics, Toronto, Canada), equipped with a 40-MHz ultrasound probe (RMV704; VisualSonics). Mice were kept under light sedation with 1–2% isoflurane until the heart rate stabilized at between 400 and 500 beats per minute. Left ventricular dimensions and wall thicknesses were determined from parasternal short-axis M-mode echocardiography images, and fractional shortening (FS) and ejection fraction (EF) were automatically calculated with Vevo 770 software.

Statistical analysis. Data are expressed as the mean ± SD. To evaluate antitumor effects, changes in body weight, and changes in cardiac function, repeated-measures ANOVA was carried out using StatView 5.0 software (Statview, Hulinks, Tokyo, Japan). Survival was assessed by the Kaplan–Meier method using SPSS version 19 software (SPSS Inc., Chicago, IL, USA). For all tests, P-values <0.05 were considered to be statistically significant. All statistical tests were two-sided.

Results

Antitumor activity of NC-6300 and epirubicin in mice bearing Hep3B s.c. tumor. NC-6300 given at 10 or 15 mg/kg three times with a 7-day interval appeared to possess significantly superior antitumor activity compared with EPI given at 10 mg/kg with the same schedule. The group treated with EPI at 10 mg/kg showed a significant decrease in body weight as compared with the groups treated with NC-6300 at 10 and 15 mg/kg (Fig. 2).

Antitumor activity of NC-6300 and epirubicin in mice bearing Hep3B/Luc liver orthotopic tumors. Antitumor activity was observed in mice bearing Hep3B/Luc xenografts implanted orthotopically following treatment with NC-6300 at 10 or 15 mg/kg or EPI at 10 mg/kg (Fig. 3). There was a significant difference between the control group and the groups treated with EPI and NC-6300 (Fig. 3b). Comparison of the relative photon count revealed significant differences between NC-6300 at 15 mg/kg and EPI at 10 mg/kg (Fig. 3b). Kaplan–Meier analysis showed that there was a significant improvement in the survival rate in the group given NC-6300 at 10 mg/kg compared with that in the group given EPI at 10 mg/kg (P = 0.002), as well as for the group given NC-6300 at 15 mg/kg compared with the group given EPI at 10 mg/kg (P = 0.004) (Fig. 3c).

Tissue distribution of NC-6300 and epirubicin in mice bearing orthotopic Hep3B/Luc tumor. Tissue distribution experiments were carried out to evaluate the toxicity and efficacy data obtained for both NC-6300 and EPI in terms of the plasma and tissue concentrations of each formulation. The concentration–time profiles in plasma and various tissues were obtained (Fig. 4) and the results were similar to previous data.[21] After the injection of EPI, its concentration declined rapidly. On the other hand, NC-6300 showed significantly slower clearance. The clearance rate of NC-6300 in orthotopic Hep3B tumors was significantly slower than that of other normal organs. In a similar manner to other drugs categorized in the drug delivery system, NC-6300 showed higher accumulation in organs of the reticuloendothelial system. In heart, a significantly higher concentration of EPI was obtained for several hours after treatment with conventional EPI compared with that of NC-6300. To compare the tissue accumulation of EPI released from NC-6300 with that of EPI after treatment with conventional EPI, the area under the time–concentration curve (AUC) values in each tissue were determined, as summarized in Table 1. NC-6300 produced increases in EPI concentration, particularly in the plasma, liver, spleen, and tumor, whereas NC-6300 decreased the free EPI concentration in kidney, lung, and heart.

Echocardiogram following treatment of NC-6300 and epirubicin. Cardiotoxicity was evaluated by echocardiography in C57BL/6 mice during and following a total of nine treatments with NC-6300 (10 mg/kg) and conventional EPI (10 mg/kg) over 12 weeks. The EF of mice treated with conventional EPI (10 mg/kg) was significantly reduced compared with those of the control (P = 0.0019) and NC-6300 (10 mg/kg) treatment groups

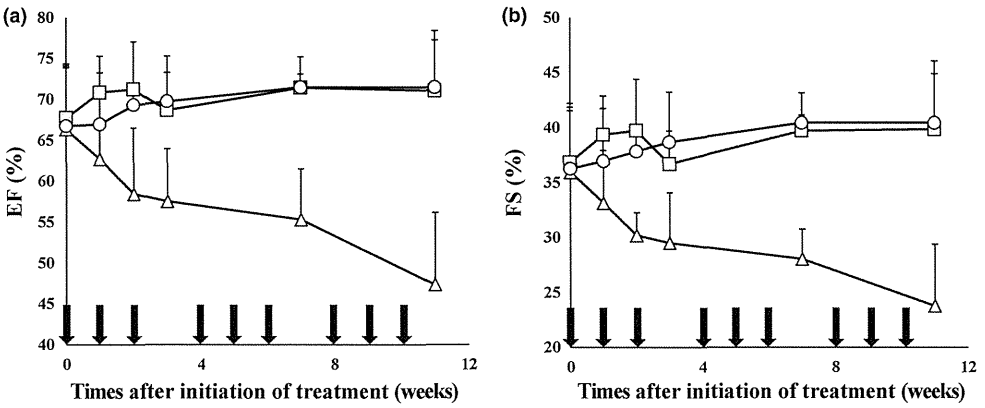

Fig. 5. Echocardiography for evaluating cardiotoxicity. C57BL/6 mice were given NC-6300 (10 mg/kg) or conventional epirubicin (EPI; 10 mg/kg) on days 0, 7, and 14 every 4 weeks, for a total of nine injections of each drug over 12 weeks (n = 6). ○, Control; □, NC-6300 at 10 mg/kg; △, EPI at 10 mg/kg. Left ventricular dimensions and wall thicknesses were determined from the echocardiography images, and ejection fraction (EF) and fractional shortening (FS) were automatically calculated. (a) Changes in EF; ANOVA test between NC-6300 (10 mg/kg) and EPI (10 mg/kg), P = 0.0081. (b) Changes in FS; ANOVA test between NC-6300 (10 mg/kg) and EPI (10 mg/kg), P = 0.0114. Arrows, drug injections; bars, SD; points, mean.

doi: 10.1111/cas.12153

($P = 0.0081$). The FS was also significantly lower in the conventional EPI treatment group (Fig. 5).

Discussion

NC-6300 was constructed to enhance antitumor activity and to reduce the adverse effects of EPI.[21] Previous data clearly showed that NC-6300 possessed superior antitumor activity to conventional EPI in mice bearing MDA-MB-231 human breast s.c. tumor.[21] In the present study, NC-6300 (10 or 15 mg/kg) also exerted significantly superior antitumor activity to EPI (10 mg/kg) both in s.c. HCC Hep3B xenografts and in the orthotopic liver tumor model. From the present pharmacokinetic analysis, we hypothesize that NC-6300 selectively accumulates in tumor tissue owing to the enhanced permeability and retention effect and directly reaches the cancer cells in order to attack them. Alternatively, the formulation spontaneously disintegrates while it is retained within the tumor tissue. Disintegrated EPI-bound unimers immediately reach and enter cancer cells. Then, under the acidic conditions in lysosomes, EPI is released to kill the cancer cells.

In terms of available preclinical data, the most prominent show that NC-6300 was found to cause marked reduction in the cardiotoxicity of conventional EPI. This was evaluated by precise echocardiography during and after a total of nine treatments with NC-6300 or EPI. The present pharmacokinetic study showed that the AUC value of released EPI in the heart was 36.2 μg h/g when NC-6300 (10 mg/kg) was given. The AUC value of EPI in the heart was 66.9 μg h/g in the case of conventional EPI treatment. The ratio of the AUC of EPI released from NC-6300 to that of native EPI was 0.54. In addition, the heart C_{max} of EPI was remarkably higher in the case of conventional EPI compared with NC-6300 treatment. In the echocardiographic examination, mice treated with conventional EPI showed significantly deteriorated EF and FS. In contrast, no mice treated with NC-6300 experienced cardiotoxicity in terms of EF and FS. Combining the results of the pharmacokinetic study and echocardiography, NC-6300 was found to markedly reduce cardiotoxicity. Among the various kinds of anticancer agents used in a clinical context, anthracyclines are one of the most important and commonly used drug groups in oncology.[9–13] Like other anticancer agents, drugs categorized into the anthracyclines have several adverse effects, including bone marrow toxicity, gastrointestinal toxicity, general fatigue, and hair loss. The most problematic adverse effect of the anthracyclines is undoubtedly cardiotoxicity[14–17] because, different from other adverse effects, it cannot be predicted when this cardiotoxicity will occur and how serious it will be. Furthermore, cardiotoxicity is occasionally unmanageable by any medical treatment. Although EPI has been developed in order to reduce the cardiotoxicity of DXR, EPI is still associated with serious cardiotoxicity.[18] However, the present data on NC-6300 suggest its potential to resolve this difficult clinical problem.

In the present preclinical study, NC-6300 appeared to show a strong antitumor effect in HCC xenografts compared with EPI. Furthermore, NC-6300 was found to reduce the cardiotoxicity of EPI markedly. Data from the present study warrant a clinical evaluation of NC-6300.

Acknowledgments

This work was supported by the Funding Program for World-Leading Innovative R&D on Science and Technology (FIRST Program) (Y.M.), the National Cancer Center Research and Development Fund (Y.M.), and the Ministry of Health, Labor and Welfare, Health and Labour Science Research Grants, Third Term Comprehensive Control Research for Cancer (Y.M.). We thank Mrs K. Shiina for her secretarial assistance.

Disclosure Statement

NanoCarrier Co. Ltd holds the patent for NC-6300 (Japanese patent number 4781435). M. Harada and H. Saito are the inventors of the product. NanoCarrier Co. Ltd received licensing fees from Kowa Co. Ltd (Nagoya, Japan) according to the license agreement.

References

1 El-Serag HB, Rudolph KL. Hepatocellular carcinoma: epidemiology and molecular carcinogenesis. *Gastroenterology* 2007; **132**: 2557–76.
2 Ferlay J, Shin HR, Bray F *et al.* Estimates of worldwide burden of cancer in 2008: GLOBOCAN 2008. *Int J Cancer* 2010; **127**: 2893–917.
3 Hung H. Treatment modalities for hepatocellular carcinoma. *Curr Cancer Drug Targets* 2005; **5**: 131–8.
4 Johnson PJ. Hepatocellular carcinoma: is current therapy really altering outcome? *Gut* 2002; **51**: 459–62.
5 Takayama T, Makuuchi M, Hirohashi S *et al.* Early hepatocellular carcinoma as an entity with a high rate of surgical cure. *Hepatology* 1998; **28**: 1241–6.
6 Llovet JM, Ricci S, Mazzaferro V *et al.* Sorafenib in advanced hepatocellular carcinoma. *N Engl J Med* 2008; **359**: 378–90.
7 Nowak AK, Chow PK, Findlay M. Systemic therapy for advanced hepatocellular carcinoma: a review. *Eur J Cancer* 2004; **40**: 1474–84.
8 Cheng AL, Kang YK, Chen Z *et al.* Efficacy and safety of sorafenib in patients in the Asia-Pacific region with advanced hepatocellular carcinoma: a phase III randomised, double-blind, placebo-controlled trial. *Lancet Oncol.* 2009; **10**: 25–34.
9 Llovet JM, Bruix J. Systematic review of randomized trials for unresectable hepatocellular carcinoma: chemoembolization improves survival. *Hepatology* 2003; **37**: 429–42.
10 Biganzoli L. Doxorubicin and paclitaxel versus doxorubicin and cyclophosphamide as first-line chemotherapy in metastatic breast cancer: The European Organization for Research and Treatment of Cancer 10961 Multicenter Phase III Trial. *J Clin Oncol* 2002; **20**: 3114–21.
11 Martin M, Rodriguez-Lescure A, Ruiz A *et al.* Randomized phase 3 trial of fluorouracil, epirubicin, and cyclophosphamide alone or followed by Paclitaxel for early breast cancer. *J Natl Cancer Inst* 2008; **100**: 805–14.
12 Roche H, Fumoleau P, Spielmann M *et al.* Sequential adjuvant epirubicin-based and docetaxel chemotherapy for node-positive breast cancer patients: the FNCLCC PACS 01 Trial. *J Clin Oncol* 2006; **24**: 5664–71.
13 Cunningham D, Starling N, Rao S *et al.* Capecitabine and oxaliplatin for advanced esophagogastric cancer. *N Engl J Med* 2008; **358**: 36–46.
14 Bristow MR, Billingham ME, Mason JW *et al.* Clinical spectrum of anthracycline antibiotic cardiotoxicity. *Cancer Treat Rep* 1978; **62**: 873–9.
15 Lefrak EA, Pitha J, Rosenheim S *et al.* A clinicopathologic analysis of adriamycin cardiotoxicity. *Cancer* 1973; **32**: 302–14.
16 Lipshultz SE, Alvarez JA, Scully RE. Anthracycline associated cardiotoxicity in survivors of childhood cancer. *Heart* 2008; **94**: 525–33.
17 Singal PK, Iliskovic N. Doxorubicin-induced cardiomyopathy. *N Engl J Med* 1998; **339**: 900–5.
18 de Azambuja E, Paesmans M, Beauduin M *et al.* Long-term benefit of high-dose epirubicin in adjuvant chemotherapy for node-positive breast cancer: 15-year efficacy results of the Belgian multicentre study. *J Clin Oncol* 2009; **27**: 720–5.
19 Salvatorelli E, Menna P, Lusini M *et al.* Doxorubicinolone formation and efflux: a salvage pathway against epirubicin accumulation in human heart. *J Pharmacol Exp Ther* 2009; **329**: 175–84.
20 Innocenti F, Iyer L, Ramirez J *et al.* Epirubicin glucuronidation is catalyzed by human UDP-glucuronosyltransferase 2B7. *Drug Metab Dispos* 2001; **29**: 686–92.
21 Harada M, Bobe I, Saito H *et al.* Improved anti-tumor activity of stabilized anthracycline polymeric micelle formulation, NC-6300. *Cancer Sci* 2011; **102**: 192–9.
22 Matsumura Y, Maeda H. A new concept for macromolecular therapeutics in cancer chemotherapy: mechanism of tumoritropic accumulation of proteins and the antitumor agent smancs. *Cancer Res* 1986; **46**: 6387–92.

SCIENTIFIC REPORTS

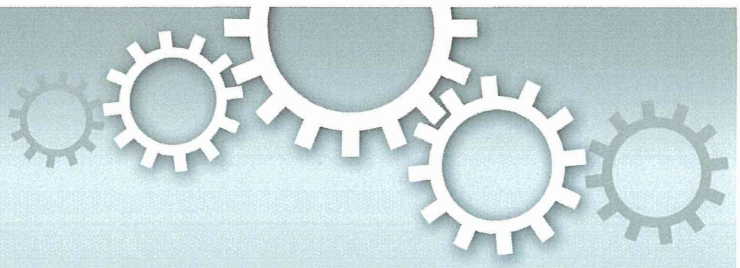

OPEN

SUBJECT AREAS:
CNS CANCER
RADIONUCLIDE IMAGING
THROMBOSIS
COAGULATION SYSTEM

Received
1 July 2013

Accepted
22 August 2013

Published
6 September 2013

Correspondence and requests for materials should be addressed to Y.M. (yhmatsum@east.ncc.go.jp)

* These authors contributed equally to this work.

Discovery of an uncovered region in fibrin clots and its clinical significance

Yohei Hisada[1,2]*, Masahiro Yasunaga[1]*, Shingo Hanaoka[3], Shinji Saijou[3], Takashi Sugino[4], Atsushi Tsuji[5], Tsuneo Saga[5], Kouhei Tsumoto[6], Shino Manabe[7], Jun-ichiro Kuroda[8], Jun-ichi Kuratsu[8] & Yasuhiro Matsumura[1,2]

[1]Division of Developmental Therapeutics, Research Centre for Innovative Oncology, National Cancer Centre Hospital East, 6-5-1 Kashiwanoha, Kashiwa, Chiba 277–8577, Japan, [2]Department of Integrated Biosciences, Graduate School of Frontier Sciences, The University of Tokyo, 5-1-5 Kashiwanoha, Kashiwa, Chiba 277–8561, Japan, [3]Project group, Biomatrix Research, Inc., 105 Higashifukai, Nagareyama, Chiba 270–0101, Japan, [4]Division of Pathology, Shizuoka Cancer Centre, 1007 Shimonagakubo, Nagaizumi, Sunto-gun, Shizuoka 411–8777, Japan, [5]Diagnostic Imaging Program, Molecular Imaging Centre, National Institute of Radiological Sciences, 4-9-1 Anagawa, Inage-ku, Chiba 263–8555, Japan, [6]Medical Proteomics Laboratory, Institute of Medical Science, The University of Tokyo, 4-6-1 Shirokanedai, Minato-ku, Tokyo 108–8639, Japan, [7]Synthetic Cellular Chemistry Laboratory, RIKEN Advanced Science Institute, 2-1 Hirosawa, Wako, Saitama 351–0198, Japan, [8]Department of Neurosurgery, Faculty of Medical and Pharmaceutical Sciences, Kumamoto University, 1-1-1 Honjo, Kumamoto, Kumamoto 860–0811, Japan.

Despite the pathological importance of fibrin clot formation, little is known about the structure of these clots because X-ray and nuclear magnetic resonance (NMR) analyses are not applicable to insoluble proteins. In contrast to previously reported anti-fibrin monoclonal antibodies (mAbs), our anti-fibrin clot mAb (clone 102–10) recognises an uncovered region that is exposed only when a fibrin clot forms. The epitope of the 102–10 mAb was mapped to a hydrophobic region on the Bβ chain that interacted closely with a counterpart region on the γ chain in a soluble state. New anti-Bβ and anti-γ mAbs specific to peptides lining the discovered region appeared to bind exclusively to fibrin clots. Furthermore, the radiolabelled 102–10 mAb selectively accumulated in mouse spontaneous tumours, and immunohistochemistry using this mAb revealed greater fibrin deposition in World Health Organization (WHO) grade 4 glioma than in lower-grade gliomas. Because erosive tumours are apt to cause micro-haemorrhages, even early asymptomatic tumours detected with a radiolabelled 102-10 mAb may be aggressively malignant.

Fibrinogen is composed of two pairs of polypeptide chains, including the Aα, Bβ, and γ chains, linked by disulfide bonds. Fibrinogen is involved in fibrin clot formation, which is the end result of blood coagulation[1–4]. Fibrin clot formation is the most dynamic and important event in haemostasis and thrombosis, which accompany injury[5], heart[6] or brain[7] infarction, severe inflammation[8], and cancer invasion[9] or metastasis[10].

Tumours that are erosive are also more destructive and thus result in fibrin clot formation. When cancer clusters erode adjacent normal or tumour vessels, micro-haemorrhage may occur, and fibrin clots are immediately formed in situ to stop the bleeding. These fibrin clots are subsequently replaced by collagenous stroma, similar to the process of normal wound healing[11]. Therefore, the "malignant cycle of blood coagulation" has been postulated to generate versatile cancer stroma, leading to cancer invasion into vessels, haemorrhage, fibrin clot formation, and replacement with collagenous tissue. Additionally, most human tumours possess abundant stroma[12,13], in contrast to human haematologic malignancies and tumour xenografts in mice, which have less interstitial tissue. Generally, more invasive cancers possess more abundant cancer stroma, most likely due to frequent haemorrhages at many places within or adjacent to the tumour tissue. In an invasive cancer, fibrin clot formation persists asymptomatically as long as cancer cells survive and expand from a tiny tumour to the advanced stage[12,13].

Results

To develop our anti-human fibrin mAb, we crushed a human fibrin clot and injected the suspension in saline into mice[13]. Consequently, we obtained a monoclonal antibody (mAb) (clone 102–10) that could distinguish fibrin clots from fibrinogen, soluble fibrin (precursor of fibrin clot[14]), and D-dimer (degradation product of fibrin clot[15]), which are all soluble proteins (Fig. 1a and Supplementary Fig. 1a). Although some anti-fibrin mAbs have been developed, none react exclusively with fibrin clots; rather, they also react with fibrinogen, soluble fibrin, or

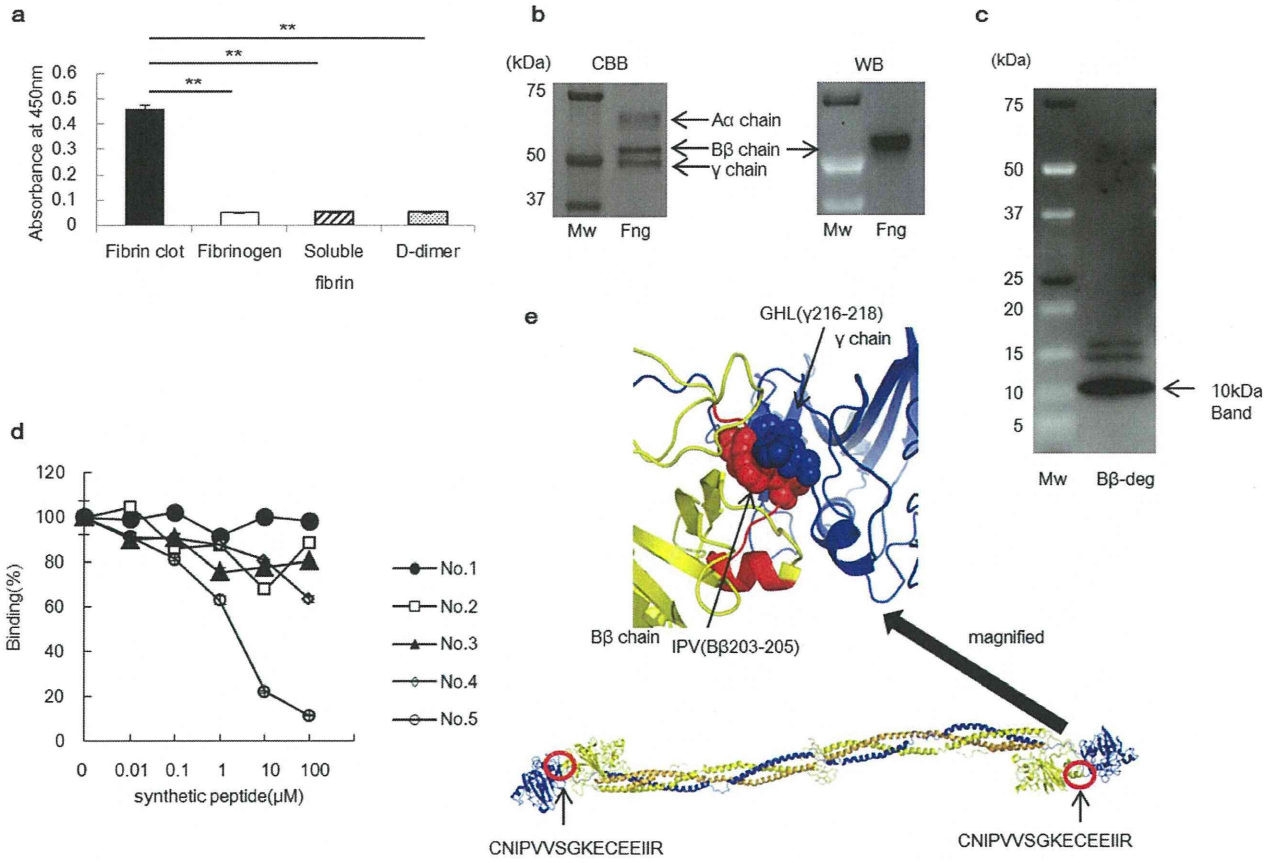

Figure 1 | Characterisation of the 102–10 mAb. (a) The 102–10 mAb was reactive to fibrin clots only ($n = 6$). The results are presented as the means ± s.d., ** $P < 0.01$. (b) Comparing CBB staining with western blot, the 102–10 mAb reacted exclusively with the Bβ chain of denatured whole fibrinogen (Fng). (c) Western blot was conducted for a sample of the digested Bβ chain, and all positive bands detected with the 102–10 mAb are shown. The amino acid sequence of the 10-kDa peptide detected by the 102–10 mAb was analysed in the next step. (d) Only the No. 5 peptide inhibited the binding of 102–10 mAb to fibrin clots ($n = 3$; $P < 0.01$, No. 4 vs. No. 5). (e) The epitope of 102–10 (Bβ201–216; red) interacted with the γ chain (blue), and Bβ203–205 (red ball) interacted with the region around γ216–218 (blue ball) in a hydrophobic manner. The whole structure of fibrinogen is shown (lower panel).

D-dimer[2,16–21]. Thus, the generation of a mAb that can distinguish fibrin clots from fibrinogen, soluble fibrin, and D-dimer represents a major breakthrough because these proteins share common amino acid sequences. The specificity of the 102–10 mAb differed from existing anti-fibrin mAbs (NYB-T2G1[22,23] and MH-1[20]), as the 102–10 mAb reacted only with fibrin clots (Supplementary Fig. 1b). Enzyme-linked immunosorbent assay (ELISA) also demonstrated that the 102–10 mAb specifically reacted with the fibrin clot in a dose-dependent manner, whereas it did not react with fibrinogen or D-dimer (Supplementary Fig. 1c).

Epitope mapping for the 102–10 mAb revealed that it reacted with fibrinogen under reducing and heat-denatured conditions in ELISA and western blot assays (Supplementary Fig. 1d–e). This result indicated that the epitope was exposed under reducing conditions. Comparing Coomassie brilliant blue (CBB) staining with the western blot results revealed that only the Bβ chain of fibrinogen reacted with the 102–10 mAb (Fig. 1b). To confirm the location of the epitope of the 102–10 mAb, the fibrinogen Bβ chain was digested with lysyl endopeptidase, and a Bβ chain derived peptide of approximately 10 kDa was obtained, which was recognised by the 102–10 mAb (Fig. 1c). According to the protein sequence result, this obtained peptide consisted of residues 149–234 of the Bβ chain. To confirm the epitope's sequence, five synthetic peptides were prepared with the following regions corresponding to synthetic peptides: No. 1 (Bβ149–178), No. 2 (Bβ179–208), No. 3 (Bβ209–234), No. 4 (Bβ171–186), and No. 5 (Bβ201–216). Competitive inhibition tests revealed that only one of these peptides (No. 5) inhibited the binding of the 102–10 mAb to fibrin clots, as measured by ELISA (Fig. 1d). The sequence of the No. 5 synthetic peptide was CNIPVVSGKECEEIIR, which constitutes a hydrophobic region of residues 201–216 of the Bβ chain. In view of the structure of fibrinogen, we could deduce that the epitope of the 102–10 mAb interacted with residues 206–220 of the γ chain of fibrinogen (Fig. 1e: Protein Data Bank (PDB) code 3GHG[24]). Interestingly, these 2 amino acid sequences are completely conserved in mammals, birds, amphibians, and fish (Basic Local Alignment Search Tool (BLAST)), which suggests that these sites have major importance for blood coagulation across species.

Identifying the epitope on a fibrin clot is generally difficult because X-ray analysis and NMR are not applicable to insoluble proteins. However, we identified the precise peptide sequence of the epitope using the 102–10 mAb against the fibrin clot and discovered a unique region in which certain sequences on the Bβ chain (containing the epitope of the 102–10 mAb) and γ chains of fibrinogen were hidden. To confirm this finding, we prepared a peptide antigen corresponding to the epitope region of the 102–10 mAb and a peptide antigen corresponding to the counterpart region on the γ chain. We immunised mice with these 2 synthetic peptides and succeeded in establishing mAbs against these regions on the Bβ chain (anti-Bβ mAb) and the γ chain (anti-γ mAb). Both the anti-Bβ mAb and the

anti-γ mAb specifically recognised fibrin clots (Fig. 2a–b). These findings imply that a conformational change occurs in the region that acts as an epitope for each mAb when fibrinogen develops into a fibrin clot, which produces the unique region (Fig. 2c). To characterise this unique region, a competition ELISA was conducted using the peroxidase-conjugated anti-Bβ mAb, peroxidase-conjugated anti-γ mAb, and each corresponding cold mAb. The binding of peroxidase-conjugated anti-Bβ mAb to the fibrin clot was blocked by the cold anti-Bβ mAb but not by the cold anti-γ mAb. Moreover, the binding of peroxidase-conjugated anti-γ mAb to the fibrin clot was blocked by the cold anti-γ mAb but not by the cold anti-Bβ mAb (Supplementary Fig. 2). These findings indicate that the newly identified unique region within fibrin clots was large enough for both the anti-Bβ and anti-γ mAbs to bind simultaneously (Fig. 2d). Further structural analysis of this unique region revealed that hydrophobic interactions and ionic and hydrogen bonds are involved in the interaction between the Bβ chain and γ chain of this particular region (Fig. 2e–g). The dynamic force exerted upon the formation of a fibrin clot is expected to break these bonds, resulting in the appearance of the unique region within the clots.

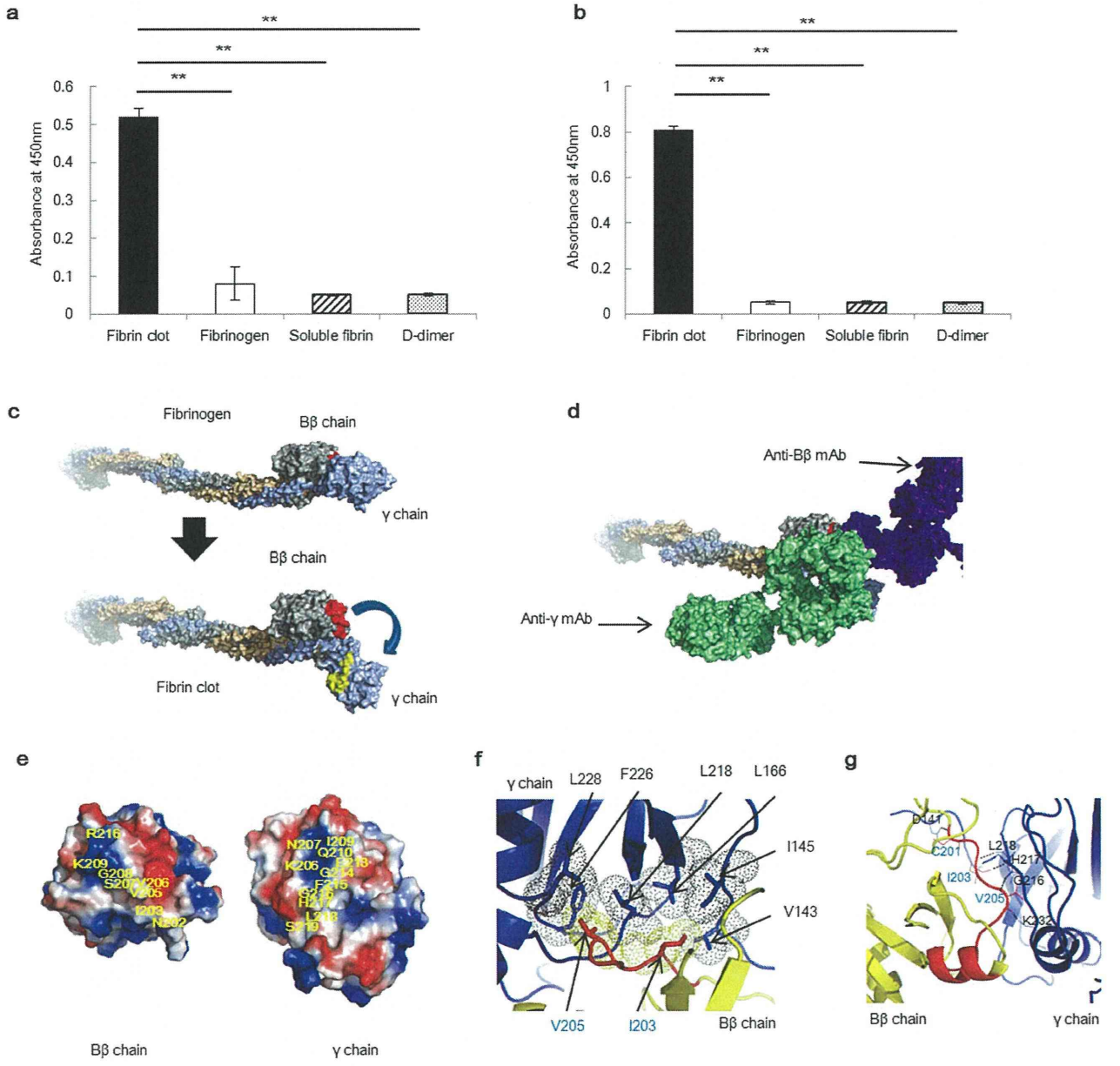

Figure 2 | Discovery of a unique region in fibrin clots. Hydrophobic, ionic, and hydrogen bonds were detected between the Bβ chain and γ chain in the unique region. (a) The anti-Bβ mAb and (b) anti-γ mAb were reactive only to fibrin clots ($n = 8$). The results are presented as the means ± s.d., ** $P < 0.01$. (c) Image of the structural change that occurred as fibrinogen transformed into a fibrin clot; the unique region was formed only when fibrinogen transformed into a fibrin clot (blue arrow). The epitope of the 102–10 mAb (red) on the Bβ chain (silver) and residues 206–220 (yellow) of the γ chain (light blue) were the components of the unique region. (d) The unique region within the fibrin clot was proposed to be large enough for both mAbs to bind to the region simultaneously. (e) Electrostatic surface representations (−5 kT/e, red, to +5 kT/e, blue) of the Bβ chain and γ chain in the unique region. Yellow characters indicate the epitope of the 102–10 mAb and the counterpart on the γ chain. (f) Hydrophobic interaction between the Bβ chain (yellow dots) and γ chain (black dots) of the unique region. (g) Amino acids (blue characters) on the Bβ chain (yellow) and amino acids (black characters) on the γ chain (blue) form hydrogen bonds in the epitope region. (f, g) Red indicates the epitope of 102–10.